Two-Wavelength Method of Measuring Path-Averaged Turbulent Surface Heat Fluxes

EDGAR L ANDREAS

U.S. Army Cold Regions Research and Engineering Laboratory, Hanover, New Hampshire

(Manuscript received 23 March 1988, in final form 31 July 1988)

ABSTRACT

Because few geophysical surfaces are horizontally homogeneous, point measurements of the turbulent surface fluxes can be unrepresentative. Path-averaging techniques are therefore desirable. This paper presents a method that yields path-averaged measurements of the sensible and latent heat fluxes with a potential accuracy as good as that for eddy-correlation measurements. The method relies on electro-optical measurements of the refractive index structure parameter C_n^2 at two wavelengths: one in the visible-to-mid-infrared region, where C_n^2 depends largely on turbulent temperature fluctuations, and a second in the near-millimeter-to-radio region, where C_n^2 depends more strongly on humidity fluctuations. A sensitivity analysis, the cornerstone of the study, provides quantitative guidelines for selecting wavelength pairs to use for the measurements. The sensitivity analysis also shows that the method is not uniformly accurate for all meteorological conditions; for limited ranges of the Bowen ratio, the sensitivity becomes so large that accurately measuring one or both heat fluxes is impossible.

1. Introduction

Eddy-correlation, inertial-dissipation, flux-gradient, or bulk-aerodynamic methods are the traditional ways of measuring the micrometeorological surface fluxes of momentum (the surface stress, τ) and sensible (H_s) and latent (H_L) heat. All yield point estimates of the fluxes. The eddy-correlation method, for example, requires direct measurements of the turbulent fluctuations in longitudinal (u) and vertical (w) velocities and in temperature (t) and absolute humidity (q); covariance calculations then yield the fluxes:

$$\tau \equiv -\rho\overline{uw} \equiv \rho u_*^2, \tag{1.1}$$

$$H_s \equiv \rho c_p \overline{wt} \equiv -\rho c_p u_* t_*, \tag{1.2}$$

$$H_L \equiv L_v \overline{wq} \equiv -L_v u_* q_*. \tag{1.3}$$

Here, ρ is the density of moist air; c_p the specific heat of air at constant pressure, L_v the latent heat of vaporization of water (or the latent heat of sublimation if the surface is frozen), and an overbar indicates an ensemble or time average. The other three methods generally yield the velocity, temperature, and humidity scales, u_*, t_*, and q_*, defined by (1.1–1.3).

Even over surfaces that are only slightly nonhomogeneous, however, point measurements of the fluxes can be unrepresentative of average surface conditions. Because nonhomogeneities are the rule rather than the exception over land and over sea ice—which is typically hummocked, ridged, and fractured—finding methods for measuring spatially averaged values of turbulent fluxes with surface-based instruments has been a goal of micrometeorologists for over two decades (Portman et al. 1962; Wesely 1976; Wyngaard and Clifford 1978).

Wesely (1976) described two optical methods for making path-averaged measurements of the heat fluxes in convective conditions. Coulter and Wesely (1980) computed path-averaged heat fluxes from measurements of the scintillation of propagating acoustic and optical waves, again in convective conditions. Kohsiek and Herben (1983) estimated latent heat flux in convective conditions solely from radio-wave scintillation. Similarly, Kohsiek (1985) suggested finding both sensible and latent heat fluxes from the scintillation of an infrared laser. An unfortunate necessity in each of these methods, however, is that all require mixing both path-averaged measurements and point measurements or making simplifying assumptions about the atmospheric stability or the statistics of temperature and humidity fluctuations. For example, optical path-averaged measurements yield an estimate of t_*. The required velocity scale u_* comes from eddy-correlation measurements of $\overline{uw}$ or from a point measurement of the mean wind speed and an assumption about the drag coefficient—a bulk-aerodynamic estimate. The latent heat flux derives from $H_L = H_s/Bo$, where the Bowen ratio $Bo = \rho c_p \Delta T / L_v \Delta Q$ comes from measurements of the vertical temperature and humidity differences, ΔT and ΔQ, at a single location.

Wyngaard and Clifford (1978) developed formulas for calculating the turbulent surface fluxes from measurements of velocity (C_v^2), temperature (C_t^2), and humidity (C_q^2) structure parameters. Kohsiek (1982a,

Corresponding author address: Dr. Edgar L Andreas, Snow and Ice Branch, Cold Regions Research and Engineering Laboratory, Corps of Engineers, Dept. of the Army, Hanover, NH 03755.

1982b) showed how to relate H_s and H_L in free convection to C_t^2 and C_q^2 and to C_{tq}, the temperature-humidity structure parameter. Turbulent refractive index fluctuations n are related to temperature and humidity fluctuations by (e.g., Andreas 1987a, 1988c)

$$n = A(\lambda, P, T, Q)t + B(\lambda, P, T, Q)q, \quad (1.4)$$

where A and B are known functions of the electromagnetic wavelength λ, the atmospheric pressure P, and the ambient temperature T and humidity Q. Therefore, the desired structure parameters are related to the refractive index structure parameter C_n^2 by

$$C_n^2 = A^2C_t^2 + B^2C_q^2 + 2ABC_{tq}. \quad (1.5)$$

Although Wyngaard and Clifford and Kohsiek suggested that path-averaging electro-optical (E–O) instruments could be used to obtain C_v^2, C_t^2, C_q^2, and C_{tq} by measuring C_n^2, they did not explain how to separate the combined effects of temperature and humidity fluctuations on C_n^2.

In this paper I describe a two-wavelength method of measuring path-averaged sensible and latent heat fluxes that overcomes the previous problems of mixing point and path-averaged measurements and of separating temperature and humidity effects on the measured parameter, C_n^2. Hill and Ochs (1983), Kohsiek and Herben (1983), and Herben and Kohsiek (1984) had anticipated this approach but discussed it only qualitatively. As I will explain later, others have solved the problem of electro-optically measuring a path-averaged value of u_*, required in (1.2) and (1.3) (Hill and Ochs 1978; Ochs and Hill 1985; Hill 1982, 1988a). I will show here how to obtain path-averaged values of t_* and q_* by using the propagation of two E–O instruments operating at distinct wavelengths; one wavelength that is sensitive primarily to turbulent temperature fluctuations, the other, to humidity fluctuations. Although the method does have an ambiguity in the signs of t_* and q_*, one way to overcome this is by using two vertically spaced E–O instruments to estimate the Obukhov length L (Andreas 1988a). Hill et al. (1988) also discussed this sign ambiguity while presenting two examples of heat fluxes estimated from C_n^2 measurements at two wavelengths.

The key element in the present work is a sensitivity study that identifies the wavelength pairs most useful for measuring t_* and q_*. I find that the best sensitivity results when an E–O device operating in the visible (to near-infrared) or in the infrared window (7.8–19 μm) is combined with a near-millimeter or radio wavelength instrument. The sensitivity analysis also shows that the measurement scheme does not have the same accuracy under all meteorological conditions. In the interval [−10, 10], two values of the Bowen ratio always exist for which the uncertainties in the measured t_* and q_* values become unacceptably large. One value depends on the quantity being estimated, t_* or q_*; the other, on ambient meteorological conditions.

2. Mathematical foundation

a. *The refractive index structure parameter*

The refractive index structure parameter C_n^2 is defined either from

$$\overline{[n(\boldsymbol{x}) - n(\boldsymbol{x} + \boldsymbol{r})]^2} = C_n^2 r^{2/3} \quad (2.1)$$

or from

$$\Phi_n(k_1) = 0.249C_n^2 k_1^{-5/3}. \quad (2.2)$$

Here $\boldsymbol{x}$ and $\boldsymbol{x} + \boldsymbol{r}$ are two points in space, r is the magnitude of the vector $\boldsymbol{r}$, Φ_n is the one-dimensional refractive index spectrum in the inertial-convective subrange, and k_1 is the one-dimensional turbulence wavenumber (e.g., Andreas 1987a).

Propagating electromagnetic (EM) waves of all wavelengths are, in one way or another, sensitive to C_n^2. Thus, a variety of electro-optical instruments has been developed to measure C_n^2. For example, for 15 yr G. R. Ochs has been designing devices called scintillometers that find path-averaged values of C_n^2 for visible or near-infrared wavelengths by measuring the scintillation (i.e., the intensity variations) of a propagating EM wave (Ochs et al. 1977; Ochs and Wang 1978; Hill and Ochs 1978; Wang et al. 1978; Ochs and Cartwright 1985). Propagation measurements using EM waves of longer wavelengths also yield C_n^2 values (Ho et al. 1978; Helmis et al. 1983; McMillan et al. 1983; Kohsiek 1982b, 1985), because the EM intensity variance is always related to a path-averaged value of C_n^2 (Lawrence and Strohbehn 1970).

It is thus assumed that we can electro-optically obtain path-averaged values of C_n^2 at several wavelengths in the visible-to-radio region. Because of technological and mathematical difficulties associated with some wavelengths, we focus on four specific EM regions: 1) visible (to near-infrared), 0.36–3 μm; 2) a mid-infrared window, 7.8–19 μm; 3) near-millimeter, 0.3–3 mm; and 4) radio waves, 3 mm and longer. The A and B values in (1.4) are different in each EM region; measuring C_n^2 in two different regions thus lets us separate the temperature and humidity contributions to refractive index fluctuations. Elsewhere I derived how the A and B values depend on λ, P, T, and Q (Andreas 1988c); appendix A summarizes those results for the four wavelength regions.

b. *Surface-layer similarity of C_n^2*

The measurement scheme developed here is good only in the atmospheric surface layer, where Monin–Obukhov similarity is valid. In the surface layer, the velocity, temperature, and humidity scales u_*, t_*, and q_* are constants with height. Using the definitions of t_* and q_*, (1.2) and (1.3), we see that on multiplying (1.4) by w, averaging, then dividing by u_*, it is also possible to define a refractive index scale that is likewise constant with height,

$$\overline{wn}/u_* \equiv n_* = At_* + Bq_*. \quad (2.3)$$

In another publication (Andreas 1988c), I showed how this scale is useful for making C_n^2 nondimensional in the surface layer and reviewed the literature relevant to this nondimensional structure parameter. It was concluded that

$$\frac{z^{2/3}C_n^2}{n_*^2} = g(\zeta), \quad (2.4)$$

where z is the measurement height, and g is a universal function that depends on the stability parameter $\zeta = z/L$. Here L is again the Obukhov length,

$$L^{-1} = \frac{\gamma\kappa}{u_*^2 T}\left(t_* + \frac{0.61T}{\rho + 0.61Q}q_*\right), \quad (2.5)$$

where γ is the acceleration of gravity, and κ is von Kármán's constant [0.4]. Implicit in (2.4) is the result $|C_{tq}| = (C_t^2 C_q^2)^{1/2}$, which is difficult to refute with the data currently available (Andreas 1987a, 1988c).

For $g(\zeta)$ in (2.4), the form with the best experimental support is the one originally proposed by Wyngaard et al. (1971), later revised by Wyngaard (1973), and modified by me to reflect a value of 0.4 for the von Kármán constant (Andreas 1988c),

$$g(\zeta) = 4.9(1 - 6.1\zeta)^{-2/3} \quad \text{for} \quad \zeta \leqslant 0, \quad (2.6a)$$

$$= 4.9(1 + 2.2\zeta^{2/3}) \quad \text{for} \quad \zeta \geqslant 0. \quad (2.6b)$$

Figure 1 shows g as a function of ζ.

The reader may be doing a double take about now. I have implied that making path-averaged E–O measurements is a remedy for the nonrepresentativeness of point measurements in mildly nonhomogeneous terrain. Yet horizontal homogeneity is fundamental to the assumptions of Monin–Obukhov similarity. That is, if we require horizontal homogeneity to analyze the path-averaged measurements, what advantage does path-averaging have? Although any proposed path-averaging system must first be tested for accuracy in horizontally homogeneous conditions, there are at least two reasons to continue exploring path-averaging techniques in nonhomogeneous terrain with the above formalism.

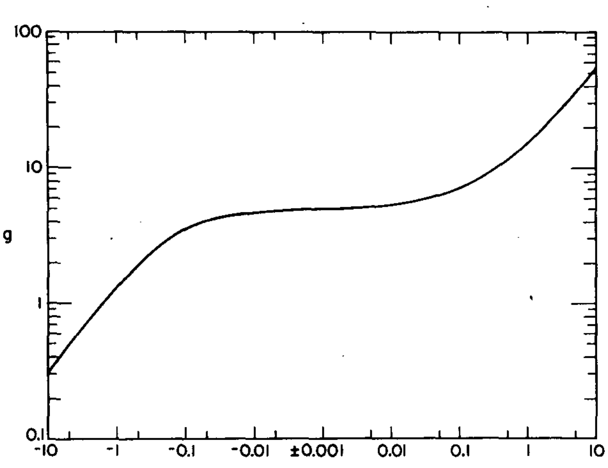

FIG. 1. The similarity function $g(\zeta)$ given by (2.6).

The first is that Monin–Obukhov similarity is the only theoretical framework we have for treating turbulence statistics in the atmospheric surface layer. We must simply try pushing it into the unknown realm of nonhomogeneous conditions and then test experimentally whether and how its predictions fail. Secondly, some experimental evidence already suggests that the predictions of Monin–Obukhov similarity are fairly accurate over nonhomogeneous surfaces. The g function in (2.4) is essentially derivable from the flux-gradient relations (Andreas 1988c)—equations expressing the surface-layer profiles of wind speed, temperature, and humidity in terms of u_*, t_*, and q_* (e.g., Businger et al. 1971; Dyer 1974; Yaglom 1977). Recent work has shown that these flux-gradient relations are accurate and thus useful even over nonuniform surfaces. Beljaars (1982) and Beljaars et al. (1983) found that they could fit velocity and temperature profiles measured in mildly nonhomogeneous terrain with existing flux-gradient relations if they used a u_* value properly reflecting some areal averaging. Smith et al. (1983) and Andreas and Murphy (1986) had good success using flux-gradient relations to explain momentum and heat transfer over Arctic leads and polynyas, surfaces that have severe thermal inhomogeneity. Using the flux-gradient relations, I also obtained reasonable fluxes over a snow field that was horizontally homogeneous in the near field (150–600 m) but had severe topographic inhomogeneities in the far field (>600 m) (Andreas 1987b). Finally, Kunkel et al. (1981) corroborated (2.4) with a $g(\zeta)$ similar to (2.6) for unstable conditions in a desert basin with "significant inhomogeneities." In summary, experimental evidence suggests that as long as a surface does not have marked undulations, extreme roughness changes, or large variations in obstacle height, judiciously applied flux-gradient relations should still model the turbulence over it, regardless of mild inhomogeneities in the surface heat and moisture fluxes. Equation (2.4) is thus justifiable for investigating path averaging in nonhomogeneous conditions.

3. Obtaining t_* and q_*

Suppose we can measure the scintillation, i.e., C_n^2, of two electromagnetic waves of wavelengths λ_1 and λ_2 propagating over coincident or close paths at height z above the surface. Each scintillation device will yield a C_n^2 value that from (2.3) and (2.4) is given by

$$C_{n_1}^2 = z^{-2/3}g(\zeta)(A_1^2 t_*^2 + B_1^2 q_*^2 + 2A_1 B_1 t_* q_*), \quad (3.1a)$$

$$C_{n_2}^2 = z^{-2/3}g(\zeta)(A_2^2 t_*^2 + B_2^2 q_*^2 + 2A_2 B_2 t_* q_*), \quad (3.1b)$$

where $A_j = A(\lambda_j, P, T, Q)$ and $B_j = B(\lambda_j, P, T, Q)$.

Take square roots of each of (3.1):

$$\frac{\mathrm{sign}_1 z^{1/3} C_{n_1}}{g^{1/2}} = A_1 t_* + B_1 q_*, \quad (3.2a)$$

$$\frac{\mathrm{sign}_2 z^{1/3} C_{n_2}}{g^{1/2}} = A_2 t_* + B_2 q_*. \quad (3.2b)$$

Here sign_1 and sign_2 remind us that the square-root operation introduces a sign ambiguity; we must set sign_1 and sign_2 to make the equalities correct.

We now see how the two-wavelength technique, at least formally, yields measurements of t_* and q_*:

$$t_* = \frac{z^{1/3}[(\mathrm{sign}_1 C_{n_1}/B_1) - (\mathrm{sign}_2 C_{n_2}/B_2)]}{g^{1/2}[(A_1/B_1) - (A_2/B_2)]}, \quad (3.3a)$$

$$q_* = \frac{z^{1/3}[(\mathrm{sign}_1 C_{n_1}/A_1) - (\mathrm{sign}_2 C_{n_2}/A_2)]}{g^{1/2}[(B_1/A_1) - (B_2/A_2)]}. \quad (3.3b)$$

Clearly, we must iterate to solve these equations, because g depends on ζ, which in turn depends on u_*, t_*, and q_*.

An earlier article (Andreas 1988a) anticipated the need for finding sign_1 and sign_2 independently of the measurements being discussed here. There I showed that by virtue of (2.4) we can estimate the Obukhov length L by measuring C_n^2 with two identical scintillometers operating over the same horizontal path, except one path is at height z_1 and the other, at height z_2. These measurements should yield the stability parameter $\tilde{\zeta} = (z_1 z_2)^{1/2}/L$ with factor-of-2 accuracy in the ranges $-3 \leq \tilde{\zeta} \leq -0.015$ and $0.02 \leq \tilde{\zeta} \leq 10$, the stability ranges most often encountered in the surface layer. Near neutral stability the method is not very accurate, but under most conditions should, at least, yield the sign of L.

Since t_* generally dominates L, these measurements give us an independent means of finding sign_1 and sign_2. Rewrite (2.5) in terms of contributions due to temperature (ζ_T) and moisture (ζ_Q) fluxes (Busch 1973):

$$\zeta = \zeta T + \zeta_Q = \frac{\gamma \kappa z t_*}{u_*^2 T}\left(1 + \frac{0.61T}{\rho + 0.61Q} \times \frac{1}{KBo}\right), \quad (3.4)$$

$$= \zeta_T\left(1 + \frac{0.61T}{\rho + 0.61Q} \times \frac{1}{KBo}\right), \quad (3.5)$$

where Bo is the Bowen ratio,

$$Bo = \frac{-\rho c_p u_* t_*}{-L_v u_* q_*} = \frac{t_*}{Kq_*}, \quad (3.6)$$

and K, for a given set of meteorological conditions, is a constant, near 2100 $\mathrm{m^3\,K\,kg^{-1}}$. From (3.4) and (3.5) we can derive

$$\frac{\zeta_Q}{\zeta_T} = \frac{0.61T}{\rho + 0.61Q} \times \frac{1}{KBo}, \quad (3.7)$$

which gives the relative importance of humidity fluctuations in determining ζ. Figure 2 plots this ratio as a function of Bo. To continue on my earlier work (Andreas 1987b, 1988c), meteorological conditions typical over a snow or sea ice surface are used here and henceforth when making computations. Therefore, for Fig. 2, P = 1000 hPa, $T = -10°\mathrm{C}$, and $Q = 1.93 \times 10^{-3}$ kg m^{-3} (i.e., relative humidity of 90%). (Here and later, none of the calculations are especially sensitive to T or Q for the range of normal atmospheric values; thus, essentially the same results would obtain at other temperatures and humidities.)

In a previous review of measurements of the Bowen ratio over snow and sea ice (Andreas 1988c), I concluded that Bo is commonly in the vicinity of -1 and 1 for snow-covered ground and for sea ice, respectively. Philip (1987) considered the Bowen ratio above both saturated and unsaturated surfaces and offered some additional guidelines on its value, none incompatible with the conclusions of my review. Figure 2 thus implies that, because ζ_Q/ζ_T is near zero for most commonly encountered values of Bo, ζ and ζ_T will almost always have the same sign. Only when $|\zeta_Q/\zeta_T| > 1$, which occurs in the interval $-0.06 < Bo < 0.06$, will ζ_Q dictate the sign of ζ. Consequently, by finding the sign of ζ, we generally know the sign of t_*.

Can we thus identify sign_1 and sign_2? Rewrite (3.2) as

$$\frac{\mathrm{sign}_1 z^{1/3} C_{n_1}}{g^{1/2}} = A_1 t_*\left(1 + \frac{B_1}{A_1 KBo}\right), \quad (3.8a)$$

$$\frac{\mathrm{sign}_2 z^{1/3} C_{n_2}}{g^{1/2}} = A_2 t_*\left(1 + \frac{B_2}{A_2 KBo}\right). \quad (3.8b)$$

Figure 3 shows a plot of the function in parentheses in (3.8) for four EM wavelengths. Again P = 1000 hPa, $T = -10°\mathrm{C}$, and $Q = 1.93 \times 10^{-3}$ kg m^{-3} were used in computing K and the A and B values (see appendix A). Without loss of generality, we can assume that in (3.8) $z^{1/3}$, C_{n_1}, C_{n_2}, and $g^{1/2}$ are all positive roots; con-

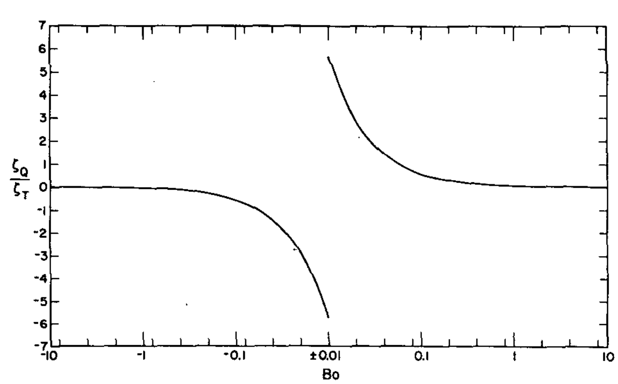

FIG. 2. ζ_Q/ζ_T, which shows the relative importance of humidity fluctuations in determining ζ, as a function of the Bowen ratio.

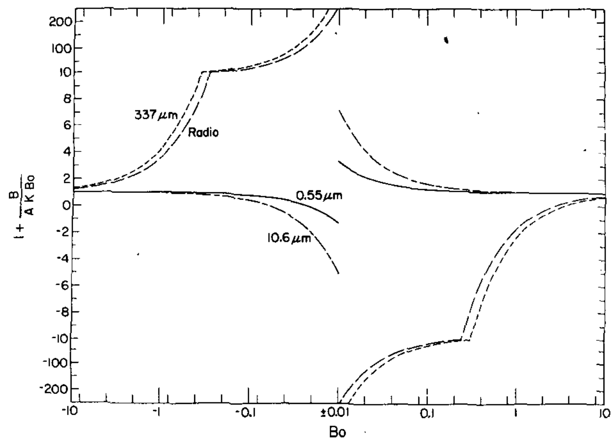

FIG. 3. The quantity $1 + B/(AKBo)$ in (3.8) as a function of the Bowen ratio. Atmospheric conditions are typical for a snow or sea ice surface: $P = 1000$ hPa, $T = -10°C$, $Q = 1.93 \times 10^{-3}$ kg m^{-3} (i.e., relative humidity of 90%). Note that the ordinate changes scale at ±10.

sequently, $sign_1$ and $sign_2$ are the same as the signs on the right-hand sides of (3.8a) and (3.8b), respectively.

From Fig. 3 we see that if $C_{n_1}^2$ is obtained from an E–O sensor operating at a wavelength that is sensitive primarily to temperature fluctuations, such as 0.55 or 10.6 μm, $1 + B/(AKBo)$ is almost always positive; $sign_1$ is thus the same as the sign of $A_1 t_*$. If $C_{n_2}^2$ comes from an E–O sensor that is especially sensitive to humidity fluctuations—i.e., near-millimeter or radio wavelengths—$sign_2$ will generally have the same sign as $A_2 t_*$ over snow-covered ground ($Bo < 0$) but may well have the opposite sign over sea ice ($Bo > 0$). If over sea ice Bo is larger than 2, which is a distinct possibility (Andreas 1988c), the signs will be the same again. Hence, over sea ice especially, some ambiguity in $sign_2$ may persist. The best way to handle this is to check whether (3.3) yields consistent estimates of t_* and q_* for the assumed values of $sign_1$ and $sign_2$ and then from t_* and q_* to compute Bo and check whether the value warrants concern over the assumptions made in interpreting Figs. 2 and 3.

An alternative way to determine $sign_1$ and $sign_2$ is to determine the signs of t_* and q_* by measuring the vertical temperature and humidity differences, ΔT and ΔQ, between two heights at a single location. Since according to Monin–Obukhov similarity the surface-layer flux is always down the gradient, ΔT and ΔQ give the signs of t_* and q_*, respectively. This procedure, unfortunately, reintroduces the problem of mixing point and path-averaged measurements, which I have been trying to avoid. Hill et al. (1988) also presented some ideas for resolving the sign ambiguity.

Although the two-wavelength method of finding t_* and q_* yields path-averaged values that should be more representative than point measurements, the measurements cannot be made any more quickly than, say, eddy-correlation measurements. Wyngaard (1973) explained that because large low-frequency eddies dominate the vertical turbulent transfer process, eddy-correlation sensors must sample several cycles of these to produce stable statistics. Eddy-correlation averaging times are, thus, nominally an hour. Since the physics of the transfer is the same regardless of the observing system, scintillometers must also sample for roughly an hour to produce physically and statistically meaningful t_* and q_* values (Andreas 1988b).

4. Sensitivity analysis

To evaluate how good (3.3a) and (3.3b) are for estimating t_* and q_*, we must know how sensitive t_* and q_* are to the required measurements of $C_{n_1}^2$, $C_{n_2}^2$, z and u_*. From (3.3a) we see that differential changes in z, ζ, C_{n_1}, and C_{n_2} produce a differential change in t_* that obeys

$$dt_* = (\partial t_*/\partial z)dz + (\partial t_*/\partial \zeta)d\zeta + (\partial t_*/\partial C_{n_1})dC_{n_1} + (\partial t_*/\partial C_{n_2})dC_{n_2}. \quad (4.1)$$

Such a differential change can be interpreted as an error in the t_* measurement resulting from measurement errors in z, ζ, $C_{n_1}^2$, or $C_{n_2}^2$. Therefore, it is more meaningful to discuss a relative change in t_* or the relative error; (4.1) thus becomes

$$\frac{dt_*}{t_*} = \frac{z}{t_*}\frac{\partial t_*}{\partial z}\frac{dz}{z} + \frac{\zeta}{t_*}\frac{\partial t_*}{\partial \zeta}\frac{d\zeta}{\zeta} + \frac{C_{n_1}}{t_*}\frac{\partial t_*}{\partial C_{n_1}}\frac{dC_{n_1}}{C_{n_1}} + \frac{C_{n_2}}{t_*}\frac{\partial t_*}{\partial C_{n_2}}\frac{dC_{n_2}}{C_{n_2}}, \quad (4.2)$$

where the terms on the right-hand side now also reflect relative errors.

Recall that ζ is a function of z, u_*, t_*, and q_*. Hence, in (4.2) we must substitute

$$\frac{\partial \zeta}{\zeta} = \frac{z}{\zeta}\frac{\partial \zeta}{\partial z}\frac{dz}{z} + \frac{u_*}{\zeta}\frac{\partial \zeta}{\partial u_*}\frac{du_*}{u_*} + \frac{t_*}{\zeta}\frac{\partial \zeta}{\partial t_*}\frac{dt_*}{t_*} + \frac{q_*}{\zeta}\frac{\partial \zeta}{\partial q_*}\frac{dq_*}{q_*}. \quad (4.3)$$

The result is

$$\left(1 - \frac{\partial t_*}{\partial \zeta}\frac{\partial \zeta}{\partial t_*}\right)\frac{dt_*}{t_*} - \frac{q_*}{t_*}\frac{\partial t_*}{\partial \zeta}\frac{\partial \zeta}{\partial q_*}\frac{dq_*}{q_*} = \frac{z}{t_*}\left(\frac{\partial t_*}{\partial z} + \frac{\partial t_*}{\partial \zeta}\frac{\partial \zeta}{\partial z}\right)\frac{dz}{z} + \frac{u_*}{t_*}\frac{\partial t_*}{\partial \zeta}\frac{\partial \zeta}{\partial u_*}\frac{du_*}{u_*} + \frac{C_{n_1}}{t_*}\frac{\partial t_*}{\partial C_{n_1}}\frac{dC_{n_1}}{C_{n_1}} + \frac{C_{n_2}}{t_*}\frac{\partial t_*}{\partial C_{n_2}}\frac{dC_{n_2}}{C_{n_2}}. \quad (4.4)$$

Notice, none of the products of partial derivatives reduces. That is, $(\partial t_*/\partial \zeta)(\partial \zeta/\partial t_*) \neq 1$, for instance, be-

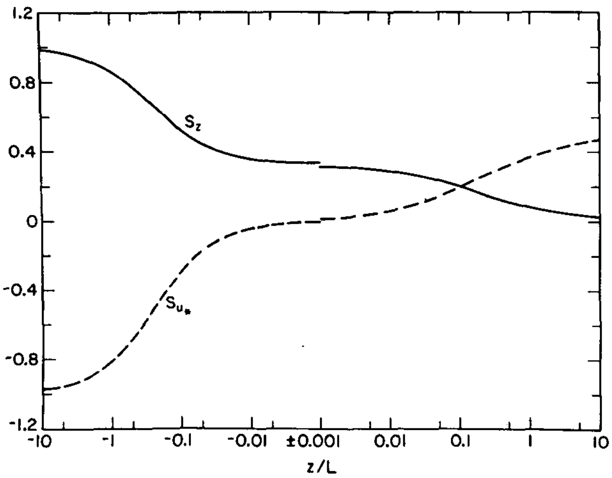

FIG. 4. The sensitivity coefficients S_z and S_{u_*} in (4.6) and (4.7) as functions of the stability.

cause (3.3a) gives the dependence of t_* on ζ $(\partial t_*/\partial \zeta)$, while (2.5) gives the dependence of ζ on t_* $(\partial \zeta/\partial t_*)$.

On inspecting (3.3b), it is easy to write down an analogous equation for q_*:

$$\left(1 - \frac{\partial q_*}{\partial \zeta}\frac{\partial \zeta}{\partial q_*}\right)\frac{dq_*}{q_*} - \frac{t_*}{q_*}\frac{\partial q_*}{\partial \zeta}\frac{\partial \zeta}{\partial t_*}\frac{dt_*}{t_*} = \frac{z}{q_*}\left(\frac{\partial q_*}{\partial z} + \frac{\partial q_*}{\partial \zeta}\frac{\partial \zeta}{\partial z}\right)\frac{dz}{z} + \frac{u_*}{q_*}\frac{\partial q_*}{\partial \zeta}\frac{\partial \zeta}{\partial u_*}\frac{du_*}{u_*} + \frac{C_{n_1}}{q_*}\frac{\partial q_*}{\partial C_{n_1}}\frac{dC_{n_1}}{C_{n_1}} + \frac{C_{n_2}}{q_*}\frac{\partial q_*}{\partial C_{n_2}}\frac{dC_{n_2}}{C_{n_2}}. \quad (4.5)$$

We can now solve (4.4) and (4.5) simultaneously for the relative errors dt_*/t_* and dq_*/q_* in terms of the relative errors in the true measured quantities z, u_*, $C_{n_1}^2$, and $C_{n_2}^2$. This derivation is finished in appendix B. The resulting sensitivity equations are

$$dt_*/t_* = S_z(dz/z) + S_{u_*}(du_*/u_*) + S_{t_1}(dC_{n_1}/C_{n_1}) + S_{t_2}(dC_{n_2}/C_{n_2}), \quad (4.6)$$

$$dq_*/q_* = S_z(dz/z) + S_{u_*}(du_*/u_*) + S_{q_1}(dC_{n_1}/C_{n_1}) + S_{q_2}(dC_{n_2}/C_{n_2}). \quad (4.7)$$

S denotes a sensitivity coefficient; appendix B gives the functional forms of these.

The meaning of sensitivity coefficients defined as in (4.6) and (4.7) has been interpreted elsewhere (Andreas 1988a). Briefly, a large S value magnifies the relative uncertainty in the measured quantity and leads to large uncertainty in the t_* or q_* measurement. A small S value, on the other hand, means that t_* or q_* is nearly independent of the measured quantity. Consequently, for predicting t_* and q_* from $C_{n_1}^2$ and $C_{n_2}^2$, optimal values for S_{t_1}, S_{t_2}, S_{q_1}, and S_{q_2} should be near 1 or −1. Then the estimated quantity is, respectively, directly or inversely proportional to the measured quantity. Of course, in practice, measurement uncertainties usually dictate acceptable sensitivity levels. With a precise measurement we can tolerate a large sensitivity coefficient; with an imprecise measurement, even a small sensitivity coefficient might lead to an unacceptably uncertain t_* or q_* estimate.

Figure 4 shows the sensitivity coefficients S_z and S_{u_*} computed from (B22), (B23), (B28), and (B29). Note that these are independent of meteorological conditions or surface parameters and, therefore, should be appropriate anywhere (2.6) and (3.1) are. According to the figure, neither S_z or S_{u_*} is ever large enough that

TABLE 1. Values of A_2B_1/A_1B_2 for the indicated wavelength pairs. Atmospheric conditions are P = 1000 hPa, T = −10°C, Q = 1.93 × 10^{-3} kg m^{-3} (i.e., relative humidity of 90%). Numbers in parentheses are A_2B_1/A_1B_2 for T = 20°C and Q = 13.9 × 10^{-3} kg m^{-3} (relative humidity of 80%) to show that the essential results demonstrated by the table do not depend strongly on T and Q.

λ_1 (μm)	λ_2 (μm) 0.55	0.94	10.6	11.4	15.0	337	2143	radio
0.55	1.00	0.97	0.38	0.34	0.21	−0.0071	−0.0088	−0.0088
			(0.38)			(−0.0107)		(−0.0123)
0.94		1.00	0.39	0.35	0.22	−0.0073	−0.0091	−0.0091
10.6			1.00	0.90	0.57	−0.019	−0.023	−0.023
						(−0.028)		(−0.033)
11.4				1.00	0.63	−0.021	−0.026	−0.026
15.0					1.00	−0.033	−0.041	−0.041
337						1.00	1.24	1.25
								(1.15)
2143							1.00	1.00
radio								1.00

uncertainty in the z or u_* measurement is detrimental to measuring t_* or q_*.

At neutral stability, $g(\zeta)^{1/2}$ in (3.3) becomes a constant, $4.9^{1/2}$; it is then simple to derive neutral-stability values for S_{t_1}, S_{t_2}, S_{q_1}, and S_{q_2}. Carrying out the mathematics, we find that the neutral-stability sensitivity coefficients are just (B12–B15)—hence, the definitions there of $S_{t_{1N}}$, $S_{t_{2N}}$, $S_{q_{1N}}$, and $S_{q_{2N}}$.

Because these neutral-stability sensitivity coefficients set the basic level of the sensitivity, it is worthwhile to consider what affects them. Each has a denominator containing the term $1 - (A_2B_1/A_1B_2)$. If we want $S_{t_{1N}}$, $S_{t_{2N}}$, $S_{q_{1N}}$, and $S_{q_{2N}}$ to be of order one, this term must not be near zero. Since the A and B values depend predominantly on the EM wavelength—and only weakly on meteorological conditions (Table 1)—optimizing this term provides a way of selecting potential wavelength pairs. Table 1 lists A_2B_1/A_1B_2 computed with the formulas in appendix A for some wavelengths that we might consider using for flux measurements. Clearly, to minimize A_2B_1/A_1B_2 we must choose wavelengths from different EM regions. For example, a visible wavelength paired with a near-millimeter or radio wavelength is a good combination; so is a wavelength from the infrared window when paired with a near-millimeter or radio wavelength.

Figure 5 reiterates these conclusions by showing $S_{t_{1N}}$, $S_{t_{2N}}$, $S_{q_{1N}}$, and $S_{q_{2N}}$ for four combinations of wavelengths. For the wavelength pairs chosen, scintillometer-1 (the 0.55 μm or 10.6 μm instrument) will provide the primary measurement of t_*, since $S_{t_{1N}}$ is near 1 for most Bowen ratios that will be encountered, while $S_{t_{2N}}$ is near zero. Scintillometer-2 (the 337 μm or radio-wavelength instrument) will provide the primary data for measuring q_*, since $S_{q_{1N}}$ is near zero for most Bowen ratios, while $S_{q_{2N}}$ is near 1. According to the figures, $|S_{t_{1N}}|$ and $|S_{t_{2N}}|$ get large as $|Bo|$ gets small; it will therefore be difficult to measure t_* accurately for small $|Bo|$. Similarly, $|S_{q_{1N}}|$ and $|S_{q_{2N}}|$ get large as $|Bo|$ gets large; measuring q_* here will be difficult. Fortunately, over snow, sea ice, the ocean at high latitude, and land surfaces with adequate soil moisture, $|Bo|$ values much below 0.1 and much above 10 are rare. Over the tropical and subtropical ocean, however, $|Bo|$ values below 0.1 are common. For measuring t_*, the pairs 0.55–337 μm and 0.55 μm-radio provide the best Bowen ratio range and the best discrimination (i.e., smallest $|S_{t_{2N}}|$). For measuring q_*, the pairs 0.55–337 μm and 10.6–337 μm are marginally better than 0.55 μm-radio and 10.6 μm-radio.

With this background we can look at the stability-dependent sensitivity coefficients given by (B24–B27). Figures 6 and 7 contain these for two wavelength pairs, 0.55–337 μm and 10.6 μm-radio. Here each sensitivity coefficient depends on $\zeta = z/L$. The figures show three situations, $\zeta = 0$, $\zeta = -1$, and $\zeta = 1$. (Clearly, the $\zeta = 0$ curve is the same one plotted for the given wave-

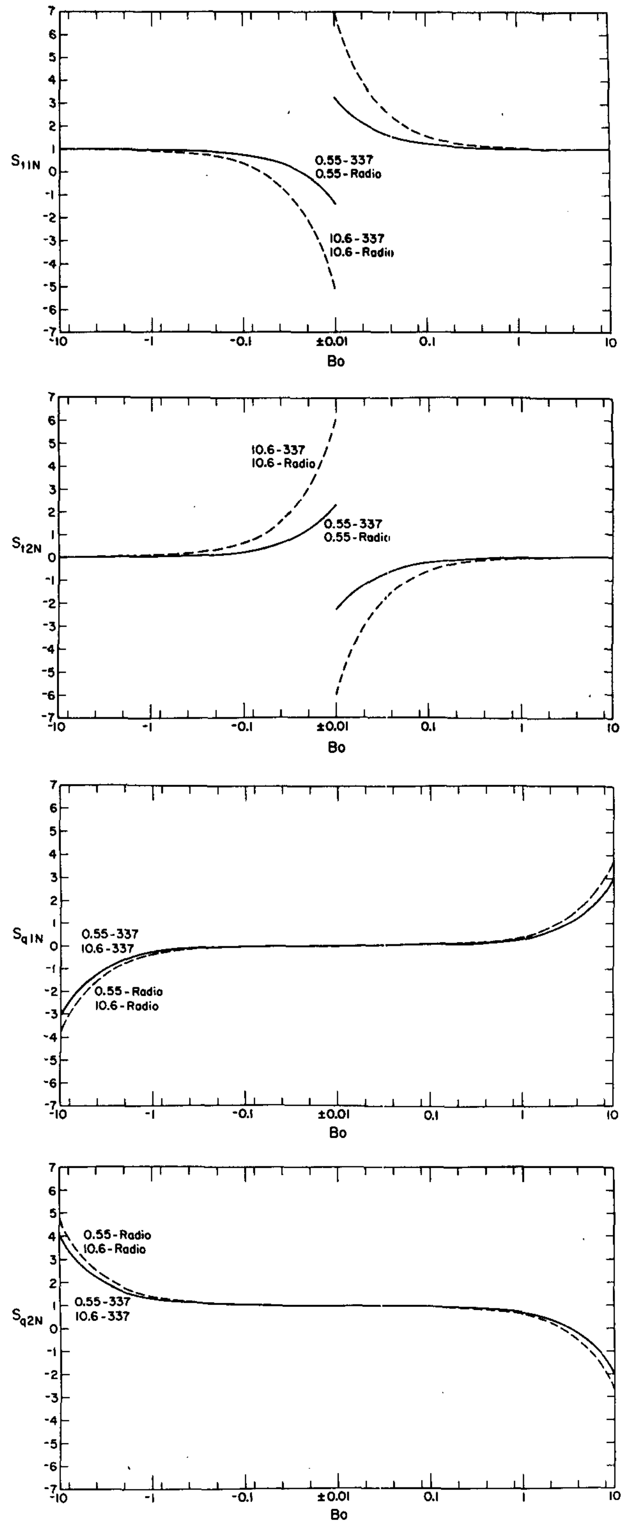

FIG. 5. The neutral-stability sensitivity coefficients $S_{t_{1N}}$, $S_{t_{2N}}$, $S_{q_{1N}}$, and $S_{q_{2N}}$, (B12–B15), for the wavelength pairs 0.55–337 μm, 0.55 μm–radio, 10.6–337 μm, and 10.6 μm–radio. Atmospheric conditions are P = 1000 hPa, T = −10°C, Q = 1.93 × 10^{-3} kg m^{-3} (i.e., relative humidity of 90%).

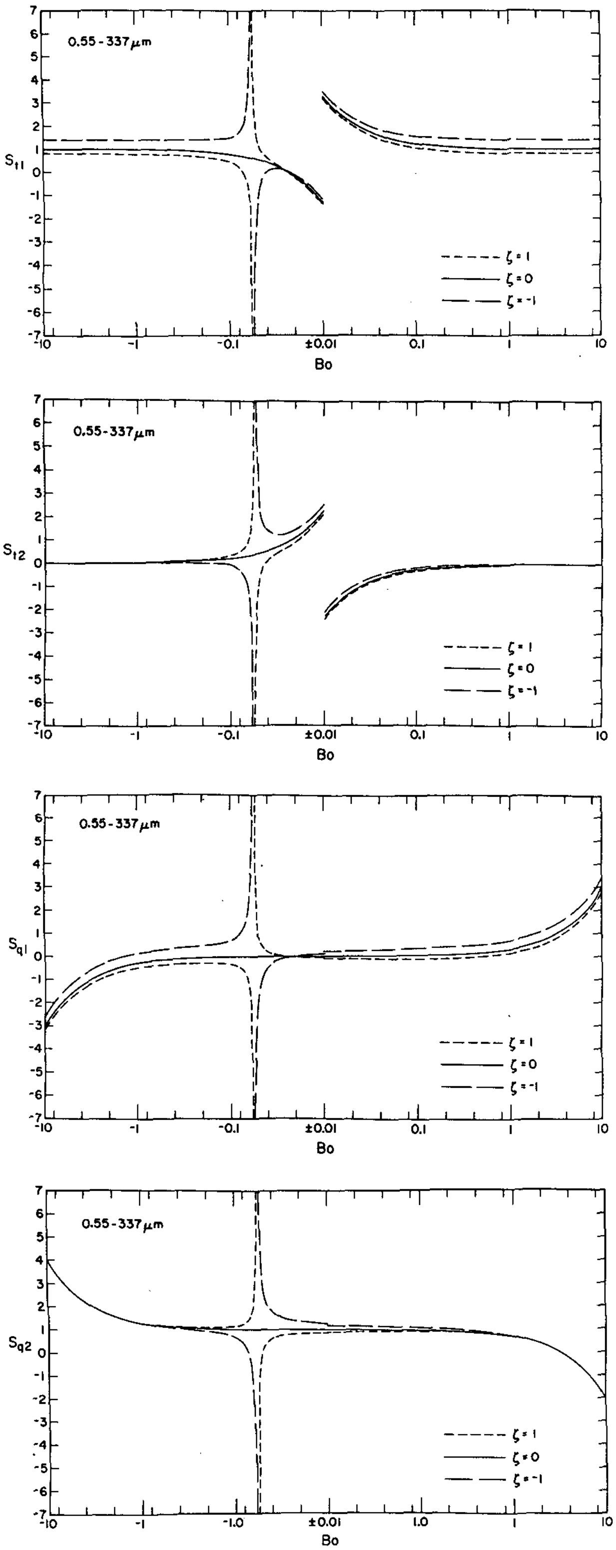

FIG. 6. The sensitivity coefficients S_{t_1}, S_{t_2}, S_{q_1}, and S_{q_2} in (4.6–4.7) for the wavelength pair 0.55–337 μm. Atmospheric conditions are $P = 1000$ hPa, $T = -10°$C, $Q = 1.93 \times 10^{-3}$ kg m^{-3} (i.e., relative humidity of 90%).

length pair in Fig. 5.) These three curves are an approximate envelope for the values of the sensitivity coefficients for all stabilities.

From Figs. 6 and 7 it is obvious that the neutral-stability values set the general level of the sensitivity coefficients; introducing stability effects alters these levels somewhat but, in general, not markedly—except near a simple pole in each function. That pole, which results because of (3.4) and (3.5), is at

$$Bo_{\text{pole}} = -0.61T/[K(\rho + 0.61Q)]. \qquad (4.8)$$

Near it, the absolute values of all the sensitivity coefficients approach infinity. Consequently, in this Bowen ratio region, measuring t_* and q_* will be impossible.

The location of the pole varies little with meteorological conditions. The Q term in (4.8) is approximately negligible in comparison to ρ; therefore, since $K = L_v/\rho c_p$, $Bo_{\text{pole}} \approx -0.61 c_p T/L_v$. Consequently, over a surface above 0°C, $Bo_{\text{pole}} \approx -2.5 \times 10^{-4}T$; over a frozen surface $Bo_{\text{pole}} \approx -2.2 \times 10^{-4}T$. Thus, between −40°C and 40°C, the very narrow pole ranges only between Bo values of −0.08 and −0.05.

In summary, Figs. 5–7 show that the two-wavelength method of measuring heat fluxes has a wide operational range but will not be accurate under all conditions. For Bowen ratios in the vicinity of the pole, which the meteorological conditions position, it will be impossible to measure either t_* or q_* accurately. For $|Bo|$ small, the accuracy of the t_* measurement degrades, with measurements based on a mid-infrared wavelength suffering more than those based on a visible or near-infrared wavelength. For $|Bo|$ large, the q_* measurement loses accuracy, with measurements based on a radio wavelength marginally worse than those based on a near-millimeter wavelength.

Finally, let us demonstrate the use of the sensitivity coefficients for estimating the uncertainty in t_* and q_* measurements. Suppose we are using the 0.55–337 μm wavelength pair (Fig. 6) and ambient conditions are those that have been used throughout, $P = 1000$ hPa, $T = -10°$C, and $Q = 1.93 \times 10^{-3}$ kg m^{-3}. Let the uncertainty in the C_{n_1} and C_{n_2} measurements be ±5% (i.e., $dC_{n_1}/C_{n_1} = dC_{n_2}/C_{n_2} = \pm 5\%$), a value certainly attainable with careful calibration (G. R. Ochs 1987, personal communication); let the uncertainties in the z and u_* measurements be ±2% and ±10%, respectively, (i.e., $dz/z = \pm 2\%$, $du_*/u_* = \pm 10\%$). Suppose the calculations or other measurements show that $z/L \approx -0.1$ and $Bo \approx -1$. From Fig. 4, $S_z = 0.5$ and $S_{u_*} = -0.3$; from Fig. 6, using the $\zeta = -1$ curve, $S_{t_1} = 1.4$, $S_{t_2} = 0$, $S_{q_1} = 0.2$, and $S_{q_2} = 1.3$. Thus, from (4.6), $dt_*/t_* = (0.5)(\pm 2\%) + (-0.3)(\pm 10\%) + (1.4)(\pm 5\%) + (0)(\pm 5\%) = \pm 11\%$ is the uncertainty in the t_* measurement. From (4.7), $dq_*/q_* = (0.5)(\pm 2\%) + (-0.3)(\pm 10\%) + (0.2)(\pm 5\%) + (1.3)(\pm 5\%) = \pm 12\%$ is the uncertainty in the q_*

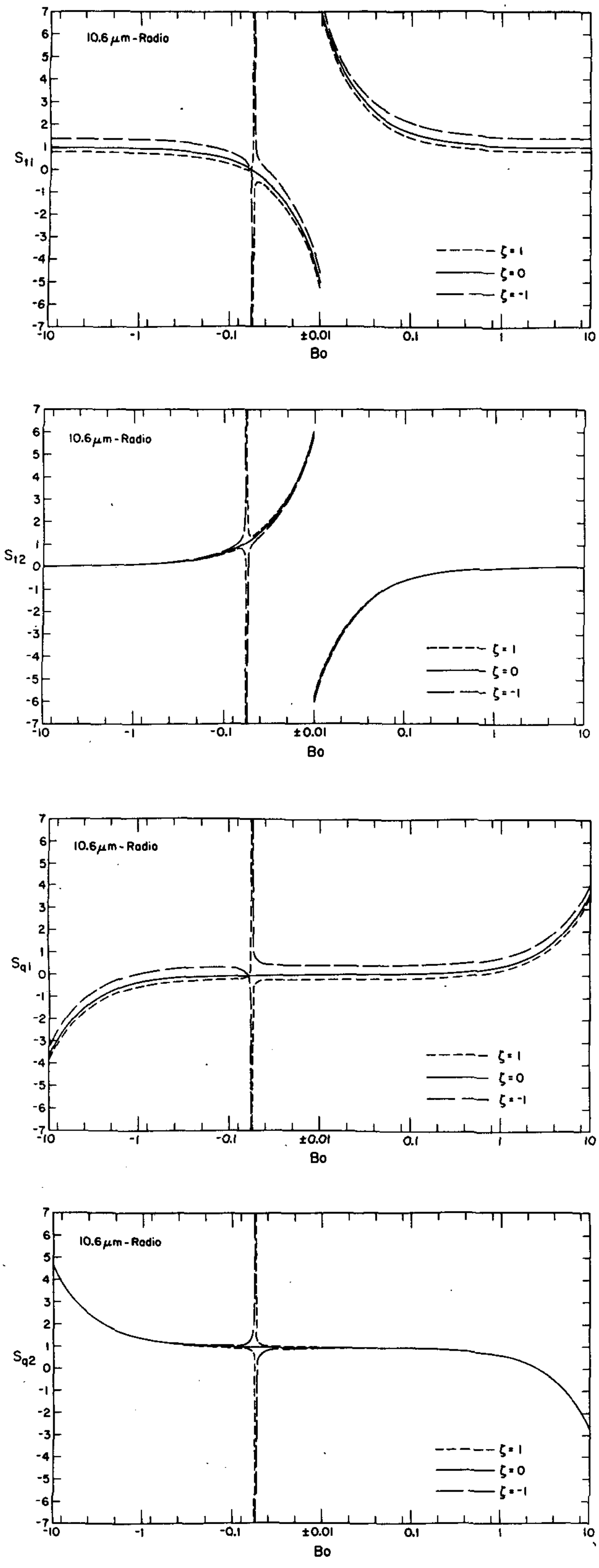

FIG. 7. As in Fig. 6, but for the wavelength pair 10.6 μm-radio.

measurement. These uncertainties are roughly what is possible with eddy-correlation measurements of the fluxes. Of course, the two-wavelength method has the advantage of yielding path-averaged fluxes.

4. Conclusion

Although the idea of making electro-optical, path-averaged measurements of the turbulent surface fluxes has been around for more than a decade, to my knowledge this is the first anyone has formally considered its potential accuracy and set down some practical guidelines.

Of primary concern is making totally path-averaged measurements at all stabilities. Others have already described how to measure a path-averaged value of u_*. Here we focused on path-averaged t_* and q_* measurements, showing that by measuring C_n^2 at two wavelengths we can separate the temperature and humidity fluxes. Although the method is ambiguous as to the signs of t_* and q_*, I had anticipated this and earlier developed a one-wavelength, two-level method for electro-optically obtaining the Obukhov length (Andreas 1988a), which usually has the same sign as t_*. Consequently, a full-blown path-averaging system requires four scintillometers, at minimum. Three are necessary to obtain t_* and q_*: two identical ones operating at wavelength λ_1 but with path heights z_1 and z_2, and a third at z_2 operating at λ_2. For obtaining u_*, we can make use of the $\lambda_1 - z_1$ scintillometer but will also need a second $\lambda_1 - z_1$ scintillometer that is different from the first either by having a smaller aperture (Hill and Ochs 1978) or a coherent light source (Ochs and Hill 1985).

A sensitivity analysis, the crux of the paper, developed an objective method for selecting λ_1 and λ_2. The best sensitivity results when a wavelength from the visible, near-infrared, or infrared-window region is paired with a near-millimeter or radio wavelength. The shorter wavelengths are sensitive primarily to turbulent temperature fluctuations, the longer wavelengths, to humidity fluctuations. From the computed sensitivity coefficients, the two-wavelength method appears to be capable of roughly the same accuracy as eddy-correlation measurements, which, when made carefully, are the most accurate of the point flux measurements (Blanc 1983, 1985).

Acknowledgments. I would like to thank R. J. Hill and G. R. Ochs for fruitful discussions and for helpful comments on the manuscript. An anonymous reviewer also provided a useful critique. The U.S. National Research Council supported me as a research associate at the NOAA Wave Propagation Laboratory in Boulder, Colorado, where I did most of this work. The U.S. Army supported me here at CRREL through Project 4A161102AT24 during the writing.

APPENDIX A

The Functions $A(\lambda, P, T, Q)$ and $B(\lambda, P, T, Q)$

It is possible to derive analytical expressions for the $A(\lambda, P, T, Q)$ and $B(\lambda, P, T, Q)$ functions defined in (1.4) for four useful wavelength regions from equations for the atmospheric refractive index set down by Bean and Dutton (1966), Owens (1967), Hill et al. (1982), Hill and Lawrence (1986), and Hill (1988b). Because those derivations are published elsewhere (Andreas 1988c), here I just summarize the functions. P, T, and Q are, respectively, the average atmospheric pressure, kelvin temperature, and absolute humidity. All quantities, including A and B, are in mks units unless stated otherwise.

a. Visible (wavelengths of 0.36–3 μm)

$$A = -10^{-6}m_1(\lambda)(P/T^2), \tag{A1}$$

$$B = 4.6150 \times 10^{-6}[m_2(\lambda) - m_1(\lambda)], \tag{A2}$$

where

$$m_1(\lambda) = 23.7134 + \frac{6839.397}{130 - \sigma^2} + \frac{45.473}{38.9 - \sigma^2}, \tag{A3}$$

$$m_2(\lambda) = 64.8731 + 0.58058\sigma^2 - 0.0071150\sigma^4 + 0.0008851\sigma^6, \tag{A4}$$

and

$$\sigma = \lambda^{-1}, \tag{A5}$$

with the wavelength λ in micrometers.

b. Infrared window (wavelengths of 7.8–19 μm)

$$A = A_{vd} + A_{iw}, \tag{A6}$$

$$B = B_{vd} + B_{iw}, \tag{A7}$$

where (A1) gives A_{vd} and

$$B_{vd} = -4.6150 \times 10^{-6}m_1(\lambda). \tag{A8}$$

For the water-vapor contributions in (A6) and (A7),

$$A_{iw} = 10^{-6}Q\{-1.359\theta^{-0.6}(\chi - 1)H^{-1} - [0.6135\theta^{-0.83} + 0.5949\theta^{-0.43}(\chi - 1)]H^{-2}\}, \tag{A9}$$

$$B_{iw} = 10^{-6}[957 - 928\theta^{0.4}(\chi - 1)]H^{-1} + 3.747/(12\,499 - \chi^2), \tag{A10}$$

where

$$\theta = T/273.16, \tag{A11}$$

$$H = 1.03\theta^{0.17} - 19.8\chi^2 + 8.2\chi^4 - 1.7\chi^8, \tag{A12}$$

$$\chi = 10/\lambda, \tag{A13}$$

with λ again in micrometers.

TABLE A1. The coefficients in (A18) and (A19).

j	α_j	a_j	β_j
1	1.382221×10^3	1.650000	0.1993324
2	-0.2135129×10^3	0.1619430	3.353494
3	-0.1485997×10^3	0.1782352	3.100942
4	-0.1088790×10^3	0.1918662	3.004944

c. Radio (wavelengths > 3 mm)

$$A = -(77.6 \times 10^{-6}P + 1.73Q)/T^2, \tag{A14}$$

$$B = 1.73/T. \tag{A15}$$

d. Near-millimeter (wavelengths of 0.3–3 mm)

$$A = A_r + A_{mw}, \tag{A16}$$

$$B = B_r + B_{mw}, \tag{A17}$$

where A_r and B_r are the nondispersive radio-wave contributions given by (A14) and (A15), respectively. The dispersive water vapor contributions to (A16) and (A17) are

$$A_{mw} = 10^{-6}(Q/T)\sum_{j=1}^{4} \alpha_j(296/T)^{a_j}(0.303/\lambda)^{2j} \times [-a_j + \beta_j(296/T)(1 + a_j)], \tag{A18}$$

$$B_{mw} = 10^{-6}\sum_{j=1}^{4} \alpha_j(296/T)^{a_j}(0.303/\lambda)^{2j} \times [1 - \beta_j(296/T)], \tag{A19}$$

where now λ is in millimeters. Table A1 gives the coefficients α_j, a_j, and β_j.

Note that because of some approximations necessary to obtain analytical expressions, (A16) and (A17) are not accurate at all wavelengths within the millimeter-wave region. In particular, because of unmodeled water vapor resonances, (A16) and (A17) should not be used in the wavelength bands 0.30–0.31 mm, 0.34–0.42 mm, and 0.44–0.83 mm.

APPENDIX B

Derivation of the Sensitivity Equations

Solving (4.4) and (4.5) for the relative errors dt_*/t_* and dq_*/q_* requires evaluating several partial derivatives. As an example, (3.3a) yields

$$\partial t_*/\partial\zeta = g(\zeta)^{1/2}t_* \frac{\partial}{\partial\zeta}[g(\zeta)^{-1/2}],$$

$$= g(\zeta)^{1/2}t_*\left[-\frac{1}{2}g(\zeta)^{-3/2}\frac{\partial g(\zeta)}{\partial\zeta}\right],$$

$$= -\frac{t_*}{2g(\zeta)}\frac{\partial g(\zeta)}{\partial\zeta}, \tag{B1}$$

and

$$\partial t_*/\partial z = t_*/3z. \tag{B2}$$

Similarly, from (3.3b) we can show

$$\partial q_*/\partial \zeta = -\frac{q_*}{2g}\frac{\partial g}{\partial \zeta}, \tag{B3}$$

$$\partial q_*/\partial z = q_*/3z. \tag{B4}$$

From (2.5),

$$\partial \zeta/\partial z = \zeta/z, \tag{B5}$$

$$\partial \zeta/\partial u_* = -2\zeta/u_*, \tag{B6}$$

$$\partial \zeta/\partial t_* = \zeta_T/t_*, \tag{B7}$$

$$\partial \zeta/\partial q_* = \zeta_Q/q_*. \tag{B8}$$

Lastly, consider the terms in (4.4) and (4.5) involving C_{n_1} and C_{n_2}. From (3.3a),

$$\frac{\partial t_*}{\partial C_{n_1}} = \frac{\mathrm{sign}_1 z^{1/3}}{g^{1/2}[(A_1/B_1) - (A_2/B_2)]B_1}. \tag{B9}$$

Or

$$\frac{C_{n_1}}{t_*}\frac{\partial t_*}{\partial C_{n_1}} = \frac{1}{1 - \dfrac{B_1}{B_2}\dfrac{\mathrm{sign}_2}{\mathrm{sign}_1}\dfrac{C_{n_2}}{C_{n_1}}}. \tag{B10}$$

From (3.8) we see that

$$\frac{B_1\,\mathrm{sign}_2 C_{n_2}}{B_2\,\mathrm{sign}_1 C_{n_1}} = \frac{1 + \dfrac{KBoA_2}{B_2}}{1 + \dfrac{KBoA_1}{B_1}}; \tag{B11}$$

therefore,

$$\frac{C_{n_1}}{t_*}\frac{\partial t_*}{\partial C_{n_1}} = \frac{1 + \dfrac{B_1}{KBoA_1}}{1 - \dfrac{A_2B_1}{A_1B_2}} \equiv S_{t_{1N}}. \tag{B12}$$

Similarly, we derive

$$\frac{C_{n_2}}{t_*}\frac{\partial t_*}{\partial C_{n_2}} = -\frac{\dfrac{A_2B_1}{A_1B_2}\left(1 + \dfrac{B_2}{KBoA_2}\right)}{1 - \dfrac{A_2B_1}{A_1B_2}} \equiv S_{t_{2N}}, \tag{B13}$$

$$\frac{C_{n_1}}{q_*}\frac{\partial q_*}{\partial C_{n_1}} = -\left(\frac{KBoA_2}{B_2}\right)\frac{C_{n_1}}{t_*}\frac{\partial t_*}{\partial C_{n_1}} \equiv S_{q_{1N}}, \tag{B14}$$

$$\frac{C_{n_2}}{q_*}\frac{\partial q_*}{\partial C_{n_2}} = -\left(\frac{KBoA_1}{B_1}\right)\frac{C_{n_2}}{t_*}\frac{\partial t_*}{\partial C_{n_2}} \equiv S_{q_{2N}}. \tag{B15}$$

Substituting (B1–B8), (B14), and (B15) into (4.4) and (4.5) gives

$$\left(1 + \frac{\zeta_T}{2g}\frac{\partial g}{\partial \zeta}\right)\frac{dt_*}{t_*} + \frac{\zeta_Q}{2g}\frac{\partial g}{\partial \zeta}\frac{dq_*}{q_*} = \left(\frac{1}{3} - \frac{\zeta}{2g}\frac{\partial g}{\partial \zeta}\right)\frac{dz}{z} + \frac{\zeta}{g}\frac{\partial g}{\partial \zeta}\frac{du_*}{u_*} + \frac{C_{n_1}}{t_*}\frac{\partial t_*}{\partial C_{n_1}}\frac{dC_{n_1}}{C_{n_1}} + \frac{C_{n_2}}{t_*}\frac{\partial t_*}{\partial C_{n_2}}\frac{dC_{n_2}}{C_{n_2}}, \tag{B16}$$

$$\left(1 + \frac{\zeta_Q}{2g}\frac{\partial g}{\partial \zeta}\right)\frac{dq_*}{q_*} + \frac{\zeta_T}{2g}\frac{\partial g}{\partial \zeta}\frac{dt_*}{t_*} = \left(\frac{1}{3} - \frac{\zeta}{2g}\frac{\partial g}{\partial \zeta}\right)\frac{dz}{z} + \frac{\zeta}{g}\frac{\partial g}{\partial \zeta}\frac{du_*}{u_*} - \left(\frac{KBoA_2}{B_2}\right)\frac{C_{n_1}}{t_*}\frac{\partial t_*}{\partial C_{n_1}}\frac{dC_{n_1}}{C_{n_1}} - \left(\frac{KBoA_1}{B_1}\right)\frac{C_{n_2}}{t_*}\frac{\partial t_*}{\partial C_{n_2}}\frac{dC_{n_2}}{C_{n_2}}. \tag{B17}$$

Solving these simultaneously for dt_*/t_* and dq_*/q_* and using (B12) and (B13) yields

$$\frac{dt_*}{t_*} = \left(1 + \frac{\zeta}{2g}\frac{\partial g}{\partial \zeta}\right)^{-1}\left\{\left(\frac{1}{3} - \frac{\zeta}{2g}\frac{\partial g}{\partial \zeta}\right)\frac{dz}{z} + \frac{\zeta}{g}\frac{\partial g}{\partial \zeta}\frac{du_*}{u_*} + \left[1 + \frac{\zeta_Q}{2g}\frac{\partial g}{\partial \zeta}\left(1 + \frac{KBoA_2}{B_2}\right)\right]S_{t_{1N}}\frac{dC_{n_1}}{C_{n_1}} + \left[1 + \frac{\zeta_Q}{2g}\frac{\partial g}{\partial \zeta}\left(1 + \frac{KBoA_1}{B_1}\right)\right]S_{t_{2N}}\frac{dC_{n_2}}{C_{n_2}}\right\}, \tag{B18}$$

$$\frac{dq_*}{q_*} = \left(1 + \frac{\zeta}{2g}\frac{\partial g}{\partial \zeta}\right)^{-1}\left\{\left(\frac{1}{3} - \frac{\zeta}{2g}\frac{\partial g}{\partial \zeta}\right)\frac{dz}{z} + \frac{\zeta}{g}\frac{\partial g}{\partial \zeta}\frac{du_*}{u_*} + \left[1 + \frac{\zeta_T}{2g}\frac{\partial g}{\partial \zeta}\left(1 + \frac{B_2}{KBoA_2}\right)\right]S_{q_{1N}}\frac{dC_{n_1}}{C_{n_1}} + \left[1 + \frac{\zeta_T}{2g}\frac{\partial g}{\partial \zeta}\left(1 + \frac{B_1}{KBoA_1}\right)\right]S_{q_{2N}}\frac{dC_{n_2}}{C_{n_2}}\right\}. \tag{B19}$$

Notice, (B18) and (B19) have several terms in common. Rewrite these as

$$dt_*/t_* = S_z(dz/z) + S_{u_*}(du_*/u_*) + S_{t_1}(dC_{n_1}/C_{n_1}) + S_{t_2}(dC_{n_2}/C_{n_2}), \tag{B20}$$

$$dq_*/q_* = S_z(dz/z) + S_{u_*}(du_*/u_*) + S_{q_1}(dC_{n_1}/C_{n_1}) + S_{q_2}(dC_{n_2}/C_{n_2}), \tag{B21}$$

where S denotes a sensitivity coefficient and

$$S_z = s_\zeta\left(\frac{1}{3} - \frac{\zeta}{2g}\frac{\partial g}{\partial \zeta}\right), \tag{B22}$$

$$S_{u_*} = s_\zeta \frac{\zeta}{g} \frac{\partial g}{\partial \zeta}, \qquad \text{(B23)}$$

$$S_{t_1} = s_\zeta \left[1 + \frac{\zeta_Q}{2g} \frac{\partial g}{\partial \zeta} \left(1 + \frac{KBoA_2}{B_2} \right) \right] S_{t_{1N}}, \qquad \text{(B24)}$$

$$S_{t_2} = s_\zeta \left[1 + \frac{\zeta_Q}{2g} \frac{\partial g}{\partial \zeta} \left(1 + \frac{KBoA_1}{B_1} \right) \right] S_{t_{2N}}, \qquad \text{(B25)}$$

$$S_{q_1} = s_\zeta \left[1 + \frac{\zeta_T}{2g} \frac{\partial g}{\partial \zeta} \left(1 + \frac{B_2}{KBoA_2} \right) \right] S_{q_{1N}}, \qquad \text{(B26)}$$

$$S_{q_2} = s_\zeta \left[1 + \frac{\zeta_T}{2g} \frac{\partial g}{\partial \zeta} \left(1 + \frac{B_1}{KBoA_1} \right) \right] S_{q_{2N}}, \qquad \text{(B27)}$$

with

$$s_\zeta = \left(1 + \frac{\zeta}{2g} \frac{\partial g}{\partial \zeta} \right)^{-1}. \qquad \text{(B28)}$$

In (B22–B28) we still need to know $g^{-1}\partial g/\partial \zeta$. From (2.6), this is

$$g^{-1} \frac{\partial g}{\partial \zeta} = \frac{\frac{2}{3}(6.1)}{1 - 6.1\zeta} \quad \text{for} \quad \zeta < 0, \qquad \text{(B29a)}$$

$$= \frac{\frac{2}{3}(2.2)}{\zeta^{1/3}(1 + 2.2\zeta^{2/3})} \quad \text{for} \quad \zeta > 0. \qquad \text{(B29b)}$$

REFERENCES

Andreas, E. L., 1987a: On the Kolmogorov constants for the temperature–humidity cospectrum and the refractive index spectrum. *J. Atmos. Sci.*, **44**, 2399–2406.

——, 1987b: Spectral measurements in a disturbed boundary layer over snow. *J. Atmos. Sci.*, **44**, 1912–1939.

——, 1988a: Atmospheric stability from scintillation measurements. *Appl. Opt.*, **27**, 2241–2246.

——, 1988b: Estimating averaging times for point and path-averaged measurements of turbulence spectra. *J. Appl. Meteor.*, **27**, 295–304.

——, 1988c: Estimating C_n^2 over snow and sea ice from meteorological data. *J. Opt. Soc. Am. A*, **5**, 481–495.

——, and B. Murphy, 1986: Bulk transfer coefficients for heat and momentum over leads and polynyas. *J. Phys. Oceanogr.*, **16**, 1875–1883.

Bean, B. R., and E. J. Dutton, 1966: *Radio Meteorology.* National Bureau of Standards Monogr. 92, U.S. Department of Commerce, 435 pp.

Beljaars, A. C. M., 1982: The derivation of fluxes from profiles in perturbed areas. *Bound.-Layer Meteor.*, **24**, 35–55.

——, P. Schotanus and F. T. M. Nieuwstadt, 1983: Surface layer similarity under nonuniform fetch conditions. *J. Climate Appl. Meteor.*, **22**, 1800–1810.

Blanc, T. V., 1983: An error analysis of profile flux, stability, and roughness length measurements made in the marine atmospheric surface layer. *Bound.-Layer Meteor.*, **26**, 243–267.

——, 1985: Variation of bulk-derived surface flux, stability, and roughness results due to the use of different transfer coefficient schemes. *J. Phys. Oceanogr.*, **15**, 650–669.

Busch, N. E., 1973: On the mechanics of atmospheric turbulence. *Workshop on Micrometeorology,* D. A. Haugen, Ed., Amer. Meteor. Soc., 1–65.

Businger, J. A., J. C. Wyngaard, Y. Izumi and E. F. Bradley, 1971: Flux-profile relationships in the atmospheric surface layer. *J. Atmos. Sci.*, **28**, 181–189.

Coulter, R. L., and M. L. Wesely, 1980: Estimates of surface heat flux from sodar and laser scintillation measurements in the unstable boundary layer. *J. Appl. Meteor.*, **19**, 1209–1222.

Dyer, A. J., 1974: A review of flux-profile relationships. *Bound.-Layer Meteor.*, **7**, 363–372.

Helmis, C. G., D. N. Asimakopoulos, C. A. Caroubalos, R. S. Cole, F. C. Medeiros Filho and D. A. R. Jayasuriya, 1983: A quantitative comparison of the refractive index structure parameter determined from refractivity measurements and amplitude scintillation measurements at 36 GHz. *IEEE Trans. Geosci. Remote Sensing,* **GE21**, 221–224.

Herben, M. H. A. J., and W. Kohsiek, 1984: A comparison of radio wave and in situ observations of tropospheric turbulence and wind velocity. *Radio Sci.*, **19**, 1057–1068.

Hill, R. J., 1982: Theory of measuring the path-averaged inner scale of turbulence by spatial filtering of optical scintillation. *Appl. Opt.*, **21**, 1201–1211.

——, 1988a: Comparison of scintillation methods for measuring the inner scale of turbulence. *Appl. Opt.*, **27**, 2187–2193.

——, 1988b: Dispersion by atmospheric water vapor at frequencies less than 1 THz. *IEEE Trans. Antennas Propag.*, **36**, 423–430.

——, and G. R. Ochs, 1978: Fine calibration of large-aperture optical scintillometers and an optical estimate of inner scale of turbulence. *Appl. Opt.*, **17**, 3608–3612.

——, and ——, 1983: Surface-layer micrometeorology by optical scintillation techniques. *Remote Probing of the Atmosphere,* Tech. Digest of the Tropical Meeting on Optical Techniques for Remote Probing of the Atmosphere, Washington, DC, Opt. Soc. of Am., TuC16.1–TuC16.4.

——, and R. S. Lawrence, 1986: Refractive index of water vapor in infrared windows. *Infrared Phys.*, **26**, 371–376.

——, —— and J. T. Priestley, 1982: Theoretical and calculational aspects of the radio refractive index of water vapor. *Radio Sci.*, **17**, 1251–1257.

——, R. A. Bohlander, S. F. Clifford, R. W. McMillan, J. T. Priestley and W. P. Schoenfeld, 1988: Turbulence-induced millimeter-wave scintillation compared with micrometeorological measurements. *IEEE Trans. Geosci. Remote Sensing,* **26**, 330–342.

Ho, K. L., N. D. Mavrokoukoulakis and R. S. Cole, 1978: Determination of the atmospheric refractive index structure parameter from refractivity measurements and amplitude scintillation measurements at 36 GHz. *J. Atmos. Terr. Phys.*, **40**, 745–747.

Kohsiek, W., 1982a: Measuring C_T^2, C_Q^2, and C_{TQ} in the unstable surface layer, and relations to the vertical fluxes of heat and moisture. *Bound.-Layer Meteor.*, **24**, 89–107.

——, 1982b: Optical and in situ measuring of structure parameters relevant to temperature and humidity, and their application to the measuring of sensible and latent heat flux. NOAA Tech. Memo. ERL WPL-96, Wave Propagation Laboratory, Boulder, 64 pp. [NTIS PB82-230533.]

——, 1985: A comparison between line-averaged observation of C_n^2 from scintillation of a CO_2 laser beam and time-averaged in situ observations. *J. Climate Appl. Meteor.*, **24**, 1099–1103.

——, and M. H. A. J. Herben, 1983: Evaporation derived from optical and radio-wave scintillation. *Appl. Opt.*, **22**, 2566–2570.

Kunkel, K. E., D. L. Walters and G. A. Ely, 1981: Behavior of the temperature structure parameter in a desert basin. *J. Appl. Meteor.*, **20**, 130–136.

Lawrence, R. S., and J. W. Strohbehn, 1970: A survey of clear-air propagation effects relevant to optical communications. *Proc. IEEE,* **58**, 1523–1545.

McMillan, R. W., R. A. Bohlander, G. R. Ochs, R. J. Hill and S. F. Clifford, 1983: Millimeter wave atmospheric turbulence measurements: Preliminary results and instrumentation for future measurements. *Opt. Eng.*, **22**, 32–39.

Ochs, G. R., and T.-I. Wang, 1978: Finite aperture optical scintillometer for profiling wind and C_n^2. *Appl. Opt.*, **17**, 3774–3778.

——, and W. D. Cartwright, 1985: Optical system model IV for space-averaged wind and C_n^2 measurements. NOAA Tech. Memo. ERL WPL-52, Revised version, Wave Propagation Laboratory, Boulder, 47 pp. [NTIS PB86-144086/XAB.]

——, and R. J. Hill, 1985: Optical-scintillation method of measuring turbulence inner scale. *Appl. Opt.*, **24**, 2430–2432.

——, R. F. Quintana and G. F. Miller, 1977: An optical device for measuring refractive index fluctuation in the atmosphere. NOAA Tech. Memo. ERL WPL-30, Wave Propagation Laboratory, Boulder, 10 pp. [NTIS AD-A051435/6GI.]

Owens, J. C., 1967: Optical refractive index of air: Dependence on pressure, temperature and composition. *Appl. Opt.*, **6**, 51–59.

Philip, J. R., 1987: A physical bound on the Bowen ratio. *J. Climate Appl. Meteor.*, **26**, 1043–1045.

Portman, D. J., F. C. Elder, E. Ryznar and V. E. Noble, 1962: Some optical properties of turbulence in stratified flow near the ground. *J. Geophys. Res.*, **67**, 3223–3235.

Smith, S. D., R. J. Anderson, G. den Hartog, D. R. Topham and R. G. Perkin, 1983: An investigation of a polynya in the Canadian Archipelago. 2, Structure of turbulence and sensible heat flux. *J. Geophys. Res.*, **88**, 2900–2910.

Wang, T.-I., G. R. Ochs and S. F. Clifford, 1978: A saturation-resistant optical scintillometer to measure C_n^2. *J. Opt. Soc. Am.*, **68**, 334–338.

Wesely, M. L., 1976: A comparison of two optical methods for measuring line averages of thermal exchanges above warm water surfaces. *J. Appl. Meteor.*, **15**, 1177–1188.

Wyngaard, J. C., 1973: On surface-layer turbulence. *Workshop on Micrometeorology*, D. A. Haugen, Ed., Amer. Meteor. Soc., 101–149.

——, and S. F. Clifford, 1978: Estimating momentum, heat and moisture fluxes from structure parameters. *J. Atmos. Sci.*, **35**, 1204–1211.

——, Y. Izumi and S. A. Collins, Jr., 1971: Behavior of the refractive-index-structure parameter near the ground. *J. Opt. Soc. Am.*, **61**, 1646–1650.

Yaglom, A. M., 1977: Comments on wind and temperature flux-profile relationships. *Bound.-Layer Meteor.*, **11**, 89–102.